Journal of Applied Physics

RESEARCH ARTICLE | AUGUST 16 2024

Improvement of tunneling magnetoresistance induced by antiferromagnetic spin orientation

Shradha Chandrashekhar Koli ; Bertrand Dupé ; Hangyu Zhou ; Weisheng Zhao

J. Appl. Phys. 136, 074901 (2024)
https://doi.org/10.1063/5.0211815

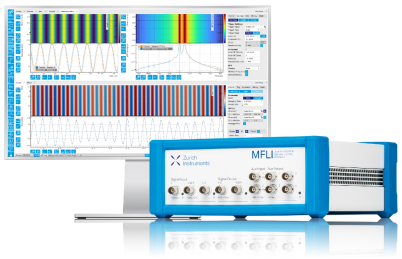

AIP Publishing

Journal of Applied Physics ARTICLE pubs.aip.org/aip/jap

Improvement of tunneling magnetoresistance induced by antiferromagnetic spin orientation

Cite as: J. Appl. Phys. **136**, 074901 (2024); doi: 10.1063/5.0211815
Submitted: 2 April 2024 · Accepted: 26 June 2024 ·
Published Online: 16 August 2024

Shradha Chandrashekhar Koli,[1,2,a)] Bertrand Dupé,[2,3,4] Hangyu Zhou,[1] and Weisheng Zhao[1,b)]

AFFILIATIONS

[1]School of Integrated Circuit Science and Engineering, MIIT Key Laboratory of Spintronics, Beihang University, Beijing 100191, China
[2]Institut fur Physik, Johannes Gutenberg Universität Mainz, D-55099 Mainz, Germany
[3]Fonds de la Recherche Scientifique (FNRS), B-1000 Brussels, Belgium
[4]Nanomat/Q-mat/CESAM, Université de Liège, B-4000 Sart Tilman, Belgium

[a)]**Electronic mail:** kshradhachandrashekhar@outlook.com
[b)]**Author to whom correspondence should be addressed:** wszhao@buaa.edu.cn

ABSTRACT

In magnetic tunnel junctions (MTJs), an antiferromagnetic iridium manganese (IrMn) layer neighboring a ferromagnetic electrode is indispensable for pinning the magnetization of the ferromagnet. The effect of its antiferromagnetism on adjacent ferromagnet and, thus, the quantum transport is, nevertheless, scarcely studied. Here, we investigate the role of antiferromagnetically orientated Mn spins in IrMn on the spin-dependent tunneling transport in IrMn/FeCo/MgO/FeCo/IrMn MTJ by analyzing the tunneling magnetoresistance (TMR) effect. The opposite spin orientation of Mn induces the mixing of Bloch symmetries, Δ_1 and Δ_5, irrespective of the spin alignment of the FeCo electrode. This auxiliary contribution from the Mn spins improves the tunneling in majority- and minority-spin channels in parallel configuration. In the antiparallel configuration, the tunneling in majority- and minority-spin channels is non-identical. The TMR as high as 8643% is obtained under equilibrium. In addition, the non-equilibrium behavior of TMR and the spin-filtering effect are examined in the voltage bias range of 10–50 mV. The TMR ratio of 3600% with the spin-filtering efficiency of ∼98% is maintained at 50 mV, presenting the MTJ as an effective spin-filtering device robust to the bias endurance. Finally, it is speculated that our device structure can be a potential spin–orbit torque-based MTJ that offers a giant TMR and promotes upscaling of the generation of multi-bit devices with a simplified design strategy.

I. INTRODUCTION

Recent advances in probing antiferromagnetic materials for the use of active elements in spintronic devices have shown that their antiferromagnetic spin orientation beneficially impacts the spin-dependent transport properties.[1–6] This effect is observed in devices employing collinear antiferromagnetic (AFM) materials. Spin-based devices incorporating collinear AFM layers have thus become a subject of interest in order to understand the role of their opposite spin orientation on transport properties. One such widely used device is the magnetic tunnel junction (MTJ) wherein a collinear IrMn is an integral layer as discussed later. MTJ is the cornerstone for reading and writing information in spin-based memory devices. Generally, it consists of an ultrathin insulating barrier sandwiched between two ferromagnetic electrodes, the relative spin alignment of which governs the high and low resistance levels leading to a tunneling magnetoresistance (TMR) effect. To accomplish this effect, the fundamental requirement is to fix the spin alignment of one of the ferromagnets, called the pinned layer, while rotating the spins of the other, called the free layer. The pinned layer, however, cannot fix its spin alignment intrinsically but requires an auxiliary antiferromagnetic layer called a pinning layer. Quite often, IrMn is chosen as the pinning layer in constructing commercial MTJs. The only function IrMn performs is to exchange couple the adjacent ferromagnet and fix its spin alignment typically by the insurgence of exchange bias effect. It was difficult to utilize IrMn or any antiferromagnet,

per se, for other practical purposes despite their favorable spin-dependent properties because of the lack of development in reading or writing of AFM spins. However, over the years, with development in controlled detection and manipulation of antiferromagnetism, IrMn has manifested itself as a potential active layer, replacing most non-magnetic heavy metals (NM-HMs).[7–9]

These NM-HMs are usually integrated in spin–orbit torque-based magnetic tunnel junctions (SOT-MTJs) as a channel layer, specifically adjacent to a free layer to switch its local magnetization direction.[10–15] SOT originating from their strong intrinsic spin–orbit coupling (SOC) generates spin currents that induce a magnetization switching through which the data are *written*. *Reading* of the data is achieved by the tunneling magnetoresistance (TMR). Typically, a major shortcoming of SOT-MTJ is its low TMR *read*-signal, and the top-pinned multilayer stacking makes it further challenging to improve.[16,17] Previous experimental reports suggest that it is advantageous to replace these NM-HM layers used to channel the SOT-*write*-current with an antiferromagnetic (AFM) metal possessing strong SOC, such as IrMn.[8,9] It can provide combined functionality such as large SOT efficiency and strong interfacial exchange coupling to manipulate the local magnetization direction. Doing so will help accomplish a field-free SOT device wherein an external magnetic field application also seems inessential. In this case, the exchange-bias field (EBF) of IrMn assists SOT-induced magnetization switching. Thus, IrMn is also being explored comprehensively as an active layer for the SOT-based device design. It is, therefore, tangible from past research advances that IrMn is a vital layer neighboring a ferromagnet in various magnetic heterostructures built to realize a wide range of magnetotransport phenomena. It can be beneficially employed as both a pinning layer neighboring a pinned layer and a channel layer neighboring a free layer. Despite its extensive application, the impact of its antiferromagnetic orientation on TMR in MTJs is less known.

The TMR effect is explained based on the symmetry-filtering theory adopted by Butler for a simple barrier model.[18] The coupling between the same type of Δ symmetry bands near the Fermi energy along the (001) direction helps the wave to propagate toward and tunnel through the MgO-barrier. Otherwise, the wave continues to decay further within the barrier itself. The rate at which the wave decays within the MgO barrier depends on the number of nodes possessed by each orbital constituent of the respective Δ symmetry.[19] As a result, any reconfiguration of *s*-derived or *d*-derived orbitals in the FM electrode will either decrease or increase the decay rate of the wave within the barrier. Now, as validated previously, when an NM-HM is incorporated in MgO-based MTJ such as NM-HM/FM/MgO/FM, the *d*-derived orbitals of FM electrode get reconfigured due to *d*–*d* hybridization between NM-HM/FeCo.[20–23] As a result, the most significant change was observed in the conductance of the minority-spin channel majorly constituted by the d-derived orbitals.

In parallel with these findings, the impact of an AFM IrMn layer on the tunneling transport is explored with anticipation that it might have a more beneficial impact on both, the majority- and minority-spin channels, compared to NM-HMs importantly because of its local AFM spin orientation. Using the first-principles method, we report improvement of TMR in a full symmetrical IrMn|FeCo|MgO|FeCo|IrMn structure. First, a vivid demonstration of this improvement is presented by studying the density of scattering states in the IrMn|FeCo|MgO|FeCo|IrMn structure (hereafter, IrMn-MTJ) and comparing it with the FeCo|MgO|FeCo structure (hereafter, FeCo-MTJ). It is found that the *s* orbital character is reconfigured by one of the Mn-atoms, which decreases the decay rate in the majority-spin channel of parallel configuration. The AFM spin orientation of Mn-atoms operates in combination with the ferromagnetic spin alignment in FeCo. By analyzing the density of local states, we show that because of the opposite and simultaneous presence of spin-up and spin-down orientation of Mn-atoms, a mixed contribution of Δ_1 and Δ_5 symmetries is observed in the majority- and minority-spin channel of parallel configuration. Furthermore, by exploring and comparing the electrostatic potential profiles, transmission probabilities in the two-dimensional Brillouin zone; the density of states along the direction of transport (z direction); and, finally, the non-equilibrium I–V curves, for parallel (P) and antiparallel (AP) configurations, it is seen that spin polarization appears in AP as well. Meanwhile, the recent experimental study in the IrMn|CoFeB|MgO structure[24] discovered that the AFM spin orientation in the IrMn channel layer and spin alignment in the adjacent CoFeB layer can be manipulated independently. Hence, switching between parallel and antiparallel spin alignments within the FeCo layers seems experimentally realizable, despite appending IrMn layers. Moreover, our structure may promote the merits essential for a promising SOT-MTJ such as (i) a purely electric-field driven device, (ii) MTJ with multiple SOT-*write*-channels, and (iii) a giant TMR ratio providing a solution to overcome the low TMR problems otherwise experienced by the SOT-MTJ.[16]

II. COMPUTATIONAL DETAILS

The IrMn|FeCo|MgO|FeCo|IrMn MTJ structure investigated in this work is a stack of five monoatomic layers (MLs) of each, along the (001) direction. It is periodic along the x- and y-direction with in-plane lattice fixed to 2.83 Å.[23,25] The out-of-plane lattice is determined by total energy relaxation. Relaxation is performed using the plane wave pseudopotential technique implemented in Vienna *Ab Initio* Simulation Package (VASP)[26] until the forces acting on each atom are smaller than 0.01 eV Å^{-1}. A k-mesh of $25 \times 25 \times 1$ and a cutoff energy of 550 eV ensured sufficient convergence of the forces.

Here, a collinear CuAu-I-type IrMn[27,28] is considered, which by far remains the material of choice in manufacturing magnetic memory devices. This binary alloy[29] belongs to D_{4h} local symmetry and $P4/mmm$ (No. 123) space group[30–32] with lattice parameters $x = y = 3.855$ Å and $z = 3.643$ Å.[33] It exists in a face-centered tetragonal (FCT) $L1_0$-structure which can be reduced to a CsCl-type B_2 structure, as shown in Fig. 1(a).[27,29] The top-view of the epitaxial interface geometry of IrMn(001)[110]‖FeCo(001)[100] is plotted in Fig. 1(b).[34,35] As a result, the in-plane lattice of B_2-IrMn is constrained to $x/\sqrt{2} = 2.73$ Å, resulting in a minimal lattice mismatch of -2.46%. The binding energy and the total free energy calculations[36] are performed in IrMn/FeCo and IrMn/FeCo/MgO stacks to inspect the interface stability. Ir–Fe termination is found energetically more favorable where Ir binds on a hollow site with Fe.

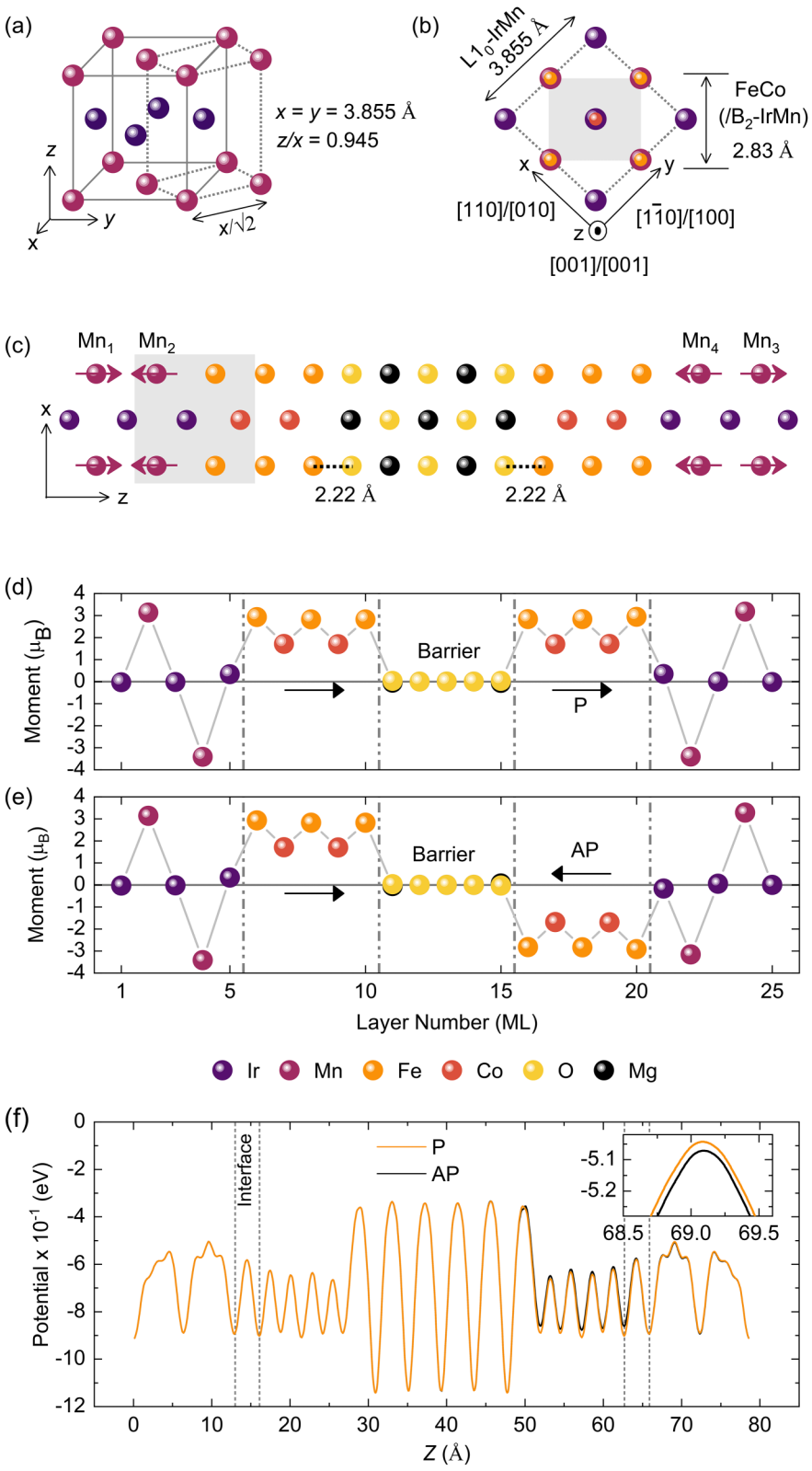

FIG. 1. (a) Crystal structure of $L1_0$-IrMn with a dashed line depicting a reduced tetragonal B_2 structure, considered in this work. (b) A crystallographic relationship of the IrMn(001)[110]/FeCo(001)[100] interface with Ir–Fe termination. (c) The total energy relaxed geometry of the central scattering region of a two-terminal IrMn-MTJ model with the numbers indicating atomic distance (in units of Å). Aubergine-colored arrows indicate the antiferromagnetic spin orientation of Mn atoms in the IrMn layer. $Mn_{1/3}$ and $Mn_{2/4}$ indicate the AFM Mn atoms' up- and down-spin orientations, respectively. The gray-colored area in (b) and (c) corresponds to the atomic arrangement immediate to the IrMn/FeCo interface. Atom- and layer-resolved magnetic moment in (d) P and (e) AP configurations. Black arrows indicate the alignment of spins within FeCo. A collinear magnetic spin alignment normal to the interface is considered. (f) The planar average of potential plotted in P and AP. The inset magnifies the difference in potential profiles of P and AP at FeCo/IrMn interface. The vertical dashed lines mark the interface. The MTJ stack is periodic along the x- and y-direction, while the transport is along the z-direction.

The quantum transport properties are calculated via the Keldysh-nonequilibrium-Green's-function formalism combined with real-space density functional theory (NEGF-DFT) as implemented in Nanodcal[37] package. The two-probe device model with the central scattering region (CSR) is shown in Fig. 1(c). The self-consistent calculation is performed using the double plus polarized (DZP) atomic orbitals basis with an electron kinetic energy cutoff of 5000 eV. During self-consistent calculations, the Hamiltonian matrix and the density matrix were converged down to less than 10^{-4} Hartree with a $k_{||}$-mesh sampling of $10 \times 10 \times 1$ for the CS region and $10 \times 10 \times 100$ for the leads. The same PBE-GGA functional was used in both structural relaxation and quantum transport calculations. The spin-decomposed conductance G_σ is given by the Landauer-Büttiker formula as,

$$G_\sigma = \frac{e^2}{h} \sum_{k_{||}} T_\sigma(k_{||}, E_F), \tag{1}$$

where $T_\sigma(k_{||}, E_F)$ is the transmission coefficient at Fermi Energy E_F with spin $\sigma = (\downarrow, \uparrow)$ and an in-plane Bloch wave vector $k_{||} = (k_x, k_y)$. e is the charge of an electron and h the Plank's constant. To evaluate the transmission coefficient and the conductance a denser $k_{||}$-mesh of $300 \times 300 \times 1$ is used for all spin channels.

The tunneling magnetoresistance (TMR) is defined as,

$$\mathrm{TMR} = \frac{G_\mathrm{P} - G_\mathrm{AP}}{G_\mathrm{AP}}, \tag{2}$$

where G_P and G_AP are the total conductance for parallel (P) and antiparallel (AP) spin alignments, respectively, within FeCo layers. Here, we consider collinear magnetic spin moments within the MTJ structure, without SOC. Figures 1(d) and 1(e) plot magnetic moments of the atoms within the central scattering region for Parallel and AP, respectively.

Next, the charge density distribution verifies a perfect matching across the boundaries between the leads (IrMn) and the central scattering region (IrMn-MTJ) as shown in Fig. S1 in the supplementary material. In addition, Fig. S2 in the supplementary material plots the sparsity patterns of the Kohn–Sham Hamiltonian matrix elements permuted to confirm the iterations of the antiferromagnetic orientation of the Mn spins. Furthermore, because IrMn and FeCo are both metallic and magnetic, understanding these layers' behavior and interfaces seems necessary. We therefore study the potential profiles for P and AP as shown in Fig. 1(f). In P, a clear uniformity is seen between the incoming (left) and outgoing (right) IrMn, FeCo, and the interfaces. On the other hand, a difference in the AP profile is seen at the outgoing (right) IrMn, FeCo, and the interfaces also magnified in the inset of Fig. 1(f). The difference in the FeCo electrodes is obvious due to the asymmetry induced by relatively opposite spin alignment while the difference in the IrMn layers seems intriguing.

TABLE I. The calculated conductance G_σ (in units of e^2h^{-1}) and the TMR ratio. $G_\mathrm{P}^{\uparrow\uparrow}$ ($G_\mathrm{P}^{\downarrow\downarrow}$) defines the spin-dependent conductance of majority (minority)-spin channel in P, while $G_\mathrm{AP}^{\uparrow\downarrow}$ ($G_\mathrm{AP}^{\downarrow\uparrow}$) defines the majority (minority)-spin channel in AP.

$G_\mathrm{P}^{\uparrow\uparrow}$	$G_\mathrm{P}^{\downarrow\downarrow}$	$G_\mathrm{AP}^{\uparrow\downarrow}$	$G_\mathrm{AP}^{\downarrow\uparrow}$	TMR
7.6×10^{-4}	2.4×10^{-5}	7.4×10^{-6}	1.6×10^{-6}	86.4

III. RESULTS AND DISCUSSION

The obtained spin-dependent conductance and TMR for IrMn-MTJ are tabulated in Table I.

We first compare the improvement of tunneling transport in IrMn-MTJ with the FeCo-MTJ by analyzing the density of scattering states (DOSSs). In an open two-terminal device, the density of scattering states (DOSS) vividly picturizes the scattering of eigenstates, per interval of energy, traveling from the left electrode ($z = -\infty$) to the right electrode ($z = +\infty$) through the central scattering region.[37] Generally, in MTJs with MgO as a barrier, the tunneling transport is dominated by Δ_1 symmetry contributing at $k_{||}$ = (0,0) in $\mathrm{P}^{\uparrow\uparrow}$ and by the resonance of interfacial states (mainly, Δ_5 symmetry) contributing at certain $k_{||} = (k_x, k_y)$ in $\mathrm{P}^{\downarrow\downarrow}$.[18] Therefore, we primarily examine the improvement at $k_{||}$ = (0,0) in $\mathrm{P}^{\uparrow\uparrow}$ and at $k_{||} = (k_x, k_y)$ in $\mathrm{P}^{\downarrow\downarrow}$. In panel (a) of Fig. 2 the scattering of Δ_1 states at $k_{||} = (0, 0)$ in $\mathrm{P}^{\uparrow\uparrow}$ shows a minor change except for

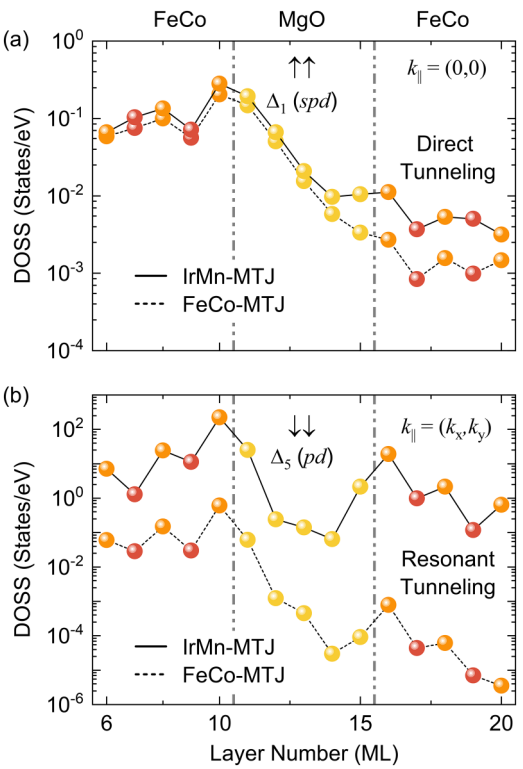

FIG. 2. Layer-resolved density of scattering states (DOSS). (a) shows Δ_1 symmetry contributing to the direct tunneling at $k_{||}$= (0,0) in the majority-spin for P. (b) shows Δ_5 symmetry contributing to the resonant tunneling in the minority-spins for P at $k_{||} = (\pm 0.25, \pm 0.37)\pi/a$ in IrMn-MTJ and $k_{||} = (\pm 0.42, \pm 0.24)\pi/a$ in FeCo-MTJ. The solid- and dashed-line indicate IrMn-MTJ and FeCo-MTJ, respectively. The vertical dashed line marks the interface.

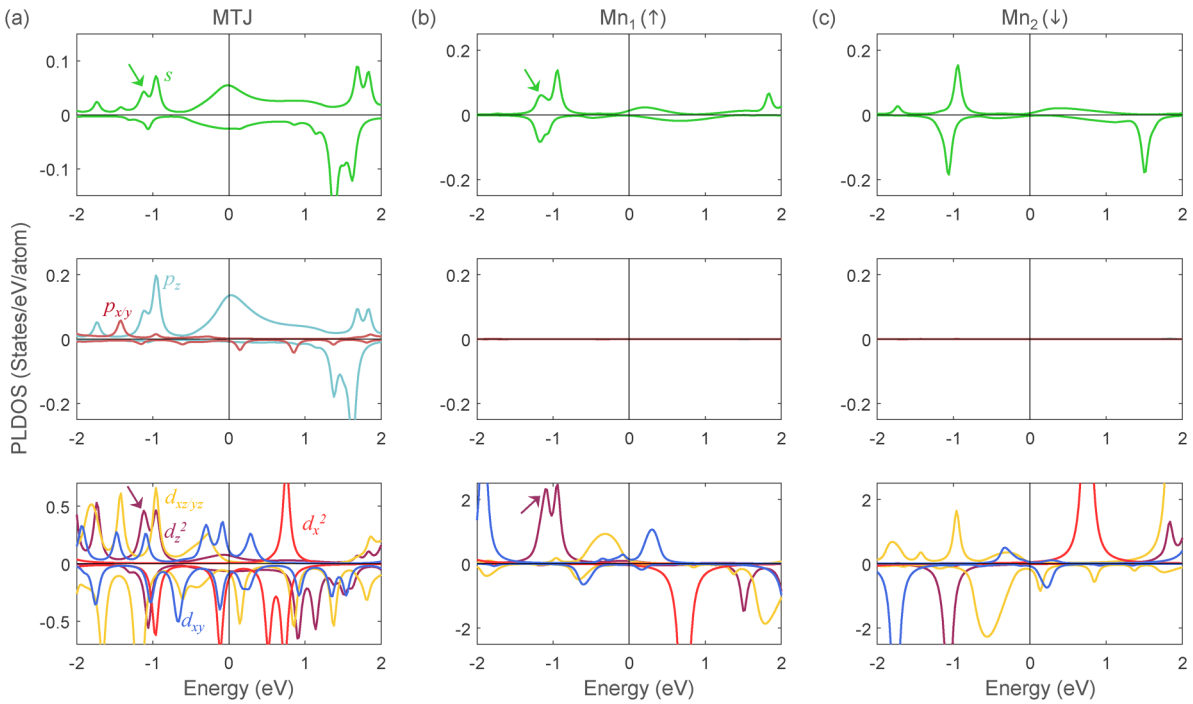

FIG. 3. Spin-resolved local density of states (a) for MTJ, (b) for $Mn_1(\uparrow)$, and (c) for $Mn_2(\downarrow)$. The green and aubergine-colored arrows highlight the shoulder to the main peak in *s* and d_z^2 orbital characters.

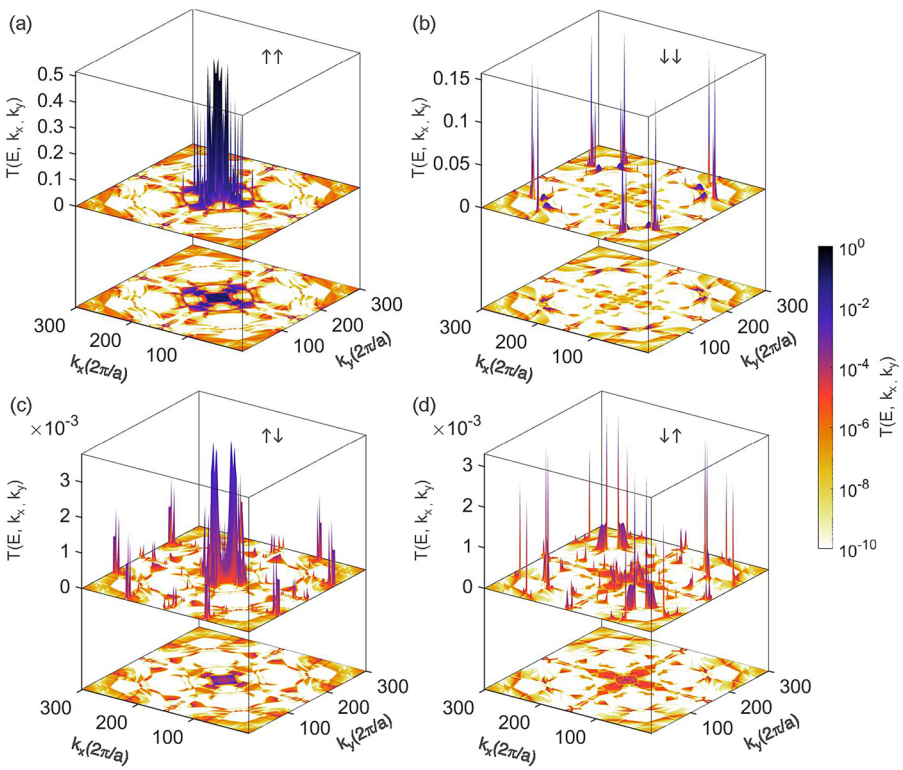

FIG. 4. $k_{\parallel}$-resolved transmission probabilities mapping on the (001)-plane of the 2D-BZ at Fermi level. (a) for majority-spin and (b) for minority-spin in P; (c) for majority-spin and (d) for minority-spin in AP. The side color bars indicate a logarithmic change in the magnitude of transmission.

the outgoing FeCo electrode and MgO/FeCo interface. The Δ_5 states at $k_{||} = (k_x, k_y)$ in $P^{\downarrow\downarrow}$ in panel (b) of Fig. 2 scatter with a significantly large difference of almost two orders of magnitude. We speculate that the cause of an increase in the interfacial states by the lattice strain on IrMn[38] also might play a role apart from the magnetic nature of IrMn. In IrMn-MTJ the resonant tunneling peaks at $k_{||} = (\pm 0.25, \pm 0.37)\pi/a$ and in FeCo-MTJ at $k_{||} = (\pm 0.42, \pm 0.24)\pi/a$.

Earlier, it has been reported that the change in the scattering of states at an outgoing interface, such as an electrode/capping interface, can be assigned to the orbital hybridization. The change at an outgoing MgO/electrode interface was not observed then and hence was not discussed.[21,23] However, in this work, the change is observed at the outgoing FeCo/IrMn and the MgO/FeCo interface, as seen in Fig. 2(a). In FeCo-MTJ, the Δ_1 states continue to decay at the same rate until they cross the interface and reach Fe-atom. On the contrary, in IrMn-MTJ, a sudden change in decay occurs almost two layers before the interface, suggesting that the IrMn layer influences the orbital hybridization at the MgO/FeCo interface as well. To confirm this phenomenon, we study the density of local states (LDOS) projected on each orbital character as shown in Fig. 3. Clearly, the s, p_z, and d_{z^2} orbitals which constitute the Δ_1 symmetry seem to have reconfigured in the MTJ in Fig. 3(a). More precisely, it is observed that a new shoulder follows the main peak at approximately -1.0 eV, originating from the Mn_1-atom (↑) [see Figs. 3(b) and 3(c)]. These Mn-atoms contribute only to the reconfiguration of s and d_{z^2} while that to the p_z is almost negligible. Nevertheless, s and d_{z^2} tend to constitute a major part of the Δ_1 symmetry in metals.[18] The p_z character is mainly reconfigured by the interfacial Fe- and O-atoms (LDOS not shown). The appearance of the shoulder to the main peak in p_z and d_{z^2} in the LDOS of MTJ in Fig. 3(a) suggest that the shoulder in d_{z^2} of Mn_1 and in p_z of interfacial

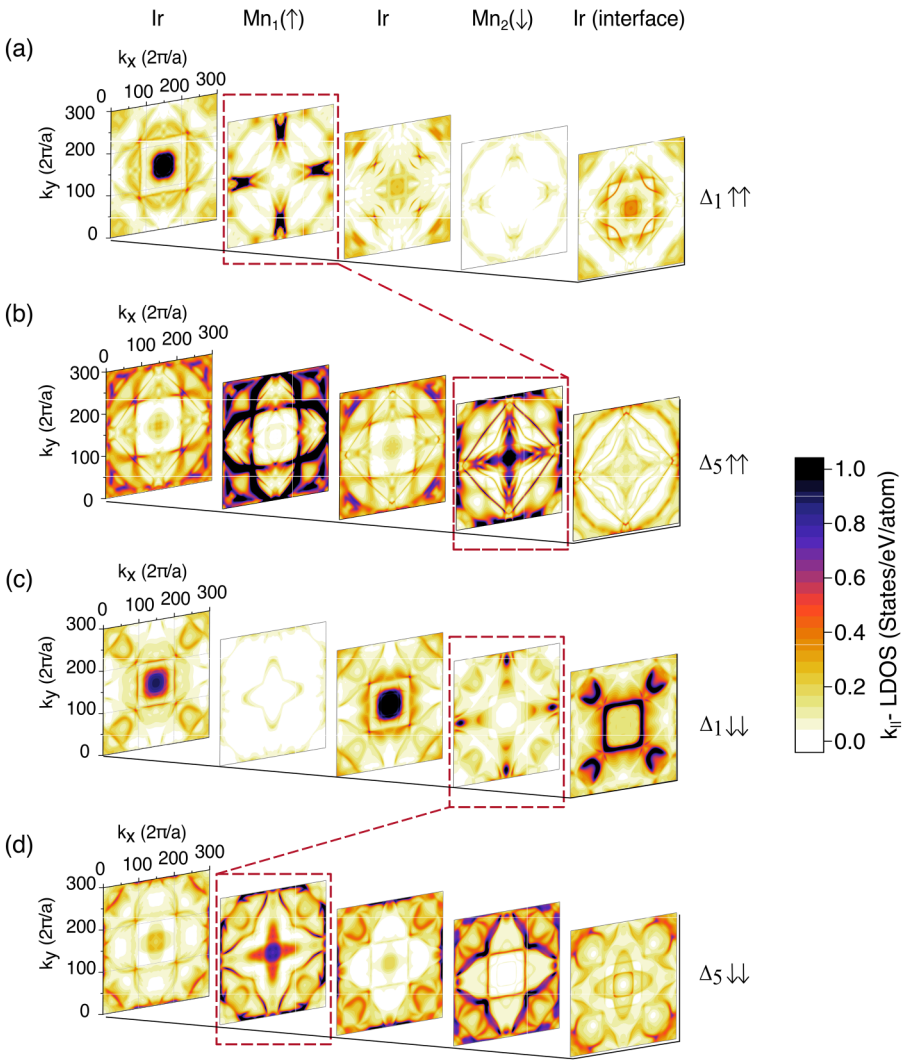

FIG. 5. $k_{||}$-resolved local density of states (LDOS) projected on each atom of the IrMn layer. (a) and (b) depict Δ_1 and Δ_5 states, respectively, for majority-spin in P. (c) and (d) depict Δ_1 and Δ_5 states, respectively, for minority-spin in P. $Mn_1(\uparrow)$ and $Mn_2(\downarrow)$ indicate the antiferromagnetic spin orientation of Mn atoms. Ir (interface) indicates the Ir atom at the IrMn/FeCo interface. The side color bar represents the distribution of LDOS on a linear scale.

atoms regulate the basic $d-p$ orbital hybridization at the MgO/FeCo interface. This regulation can explain the change in the decay rate of Δ_1 state at the outgoing interfacial O–Fe atoms. On the other hand, the minor change in the decay rate within the MgO-barrier might originate from the reconfiguration of the s orbital. The decay rate within the MgO-barrier depends on the number of nodes in the orbital character. Therefore, any modification in s-derived character should assist in lowering the decay rate.[19] It is important to note is that only one of the Mn-atoms, i.e., Mn_1 that favors the local spin-orientation of the adjacent FeCo electrode contributes to the shoulder peak, whereas Mn_2 with opposite local spin-orientation does not. This proves that the reconfiguration of the Δ_1 state is associated with the magnetic property of Mn atoms in the IrMn layer and not with the material property.

The discussion of the preceding paragraphs applies to the tunneling at only specific points in the $k_\parallel$-space, i.e., at $k_\parallel$ = (0,0) in $P^{\uparrow\uparrow}$ and $k_\parallel = (k_x, k_y)$ in $P^{\downarrow\downarrow}$, to provide a compendious demonstration of an improvement in transmission after incorporating IrMn layers. However, it should be emphasized that the tunneling transmission is an integration over all $k_\parallel$-points in the two-dimensional Brillouin zone (2DBZ) at Fermi energy (E_F) for every spin channel. To understand the microscopic behavior, the transmission probability as a function of $k_\parallel$-space for P and AP alignments of FeCo electrodes are studied [see Figs. 4(a)–4(d)]. In Fig. 4(a), for $P^{\uparrow\uparrow}$, a remarkably high peak at $k_\parallel$ = (0,0) is accompanied by multiple other high peaks close to $k_\parallel$ = (0,0). This indicates that the large transmission at and around $k_\parallel$ = (0,0) might not be entirely dominated by Δ_1 symmetry but is also contributed by other symmetries. Δ_1 symmetry typically exhibits a single and broad Gaussian-like peak at $k_\parallel$ = (0,0).[18] This symmetry mixing, however, does not tend to disturb the direct (coherent) tunneling through the MgO barrier, which is confirmed by the high peak at $k_\parallel$ = (0,0). The transmission for $P^{\downarrow\downarrow}$ in [Fig. 4(b)] is dominated by the sharp resonant peaks (hot-spots) at $k_\parallel = (\pm 0.25, \pm 0.37)\pi/a$, reminiscent of what happens in FeCo-MTJ. However, the transmission at and close to $k_\parallel$ = (0,0) is not relatively negligible. For $AP^{\uparrow\downarrow}$ and $AP^{\downarrow\uparrow}$, the transmission is completely non-identical as seen in Figs. 4(c) and 4(d).

Before moving on to the non-identical characteristics of the transmission for AP alignment, we discuss the occurrence of symmetry-mixing for P alignment. Figures 5(a)–5(d) summarize the symmetry-resolved local density of states in $k_\parallel$-space projected on each atom of the IrMn layer. The mixing of symmetry (Δ_1 and Δ_5) is mostly visible in antiferromagnetically oriented Mn atoms. The conspicuous distribution of the states of the Mn-atoms suggests that the contribution from Δ_1 states of Mn_1 and Δ_5 states of Mn_2 coexist in either $P^{\uparrow\uparrow}$ or $P^{\downarrow\downarrow}$ channel. Alternatingly, when one type of symmetry state exhibits dominance at $k_\parallel$ = (0,0), the other exhibits far away from $k_\parallel$ = (0,0). Panels (a) and (b) in Fig. 5 show that Δ_1 states of Mn_1 are mostly concentrated close to X-point, while Δ_5 states of Mn_2 are concentrated at the Γ-point and on the Γ-X line. The pattern

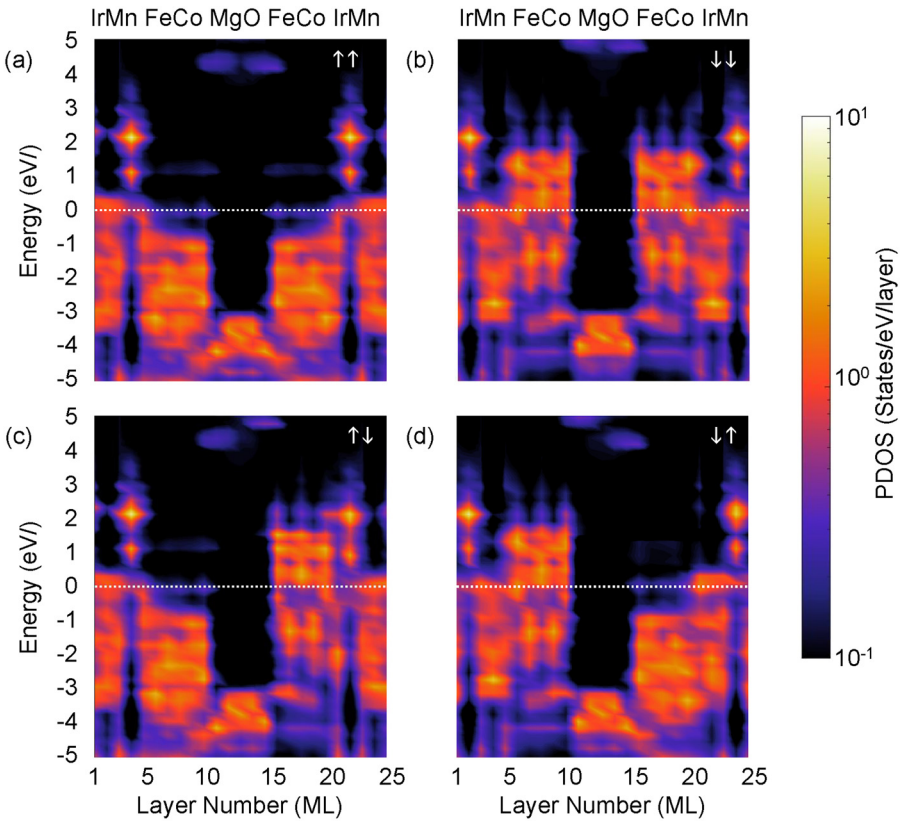

FIG. 6. Projected density of states (PDOS) along the direction of transport (z-direction). (a)–(b) for P and (c)–(d) for AP. The side color bar indicates the occupation of PDOS on a logarithm scale.

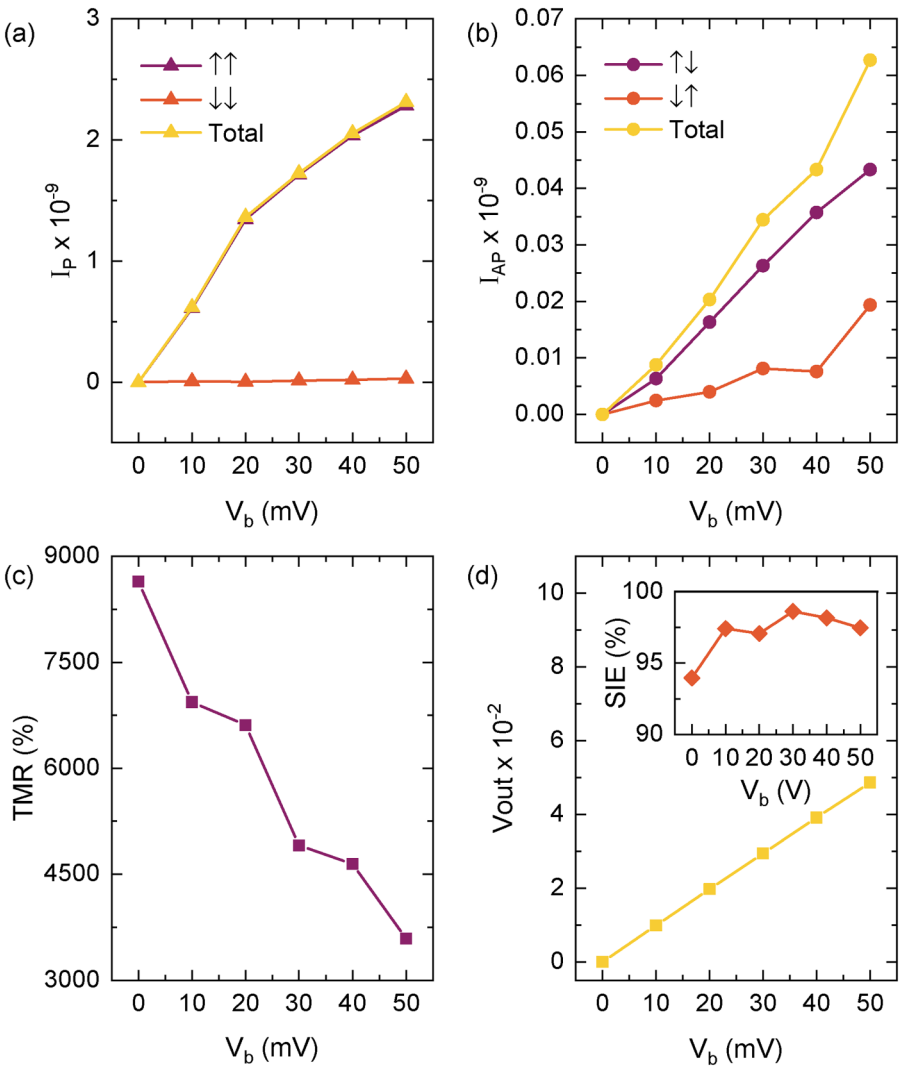

FIG. 7. Non-equilibrium characteristics of tunneling for bias voltage V_b. (a) and (b) plot *I–V* curves for P and AP, respectively. (c) TMR and (d) the output signal V_{out} with spin-filtering efficiency for P (inset).

displayed by the distribution of Δ_5 states of Mn_2 in panels (b) and (c) resembles the transmission pattern in panels (a) and (b) of Fig. 5, close to $k_{\|}$= (0,0). Strikingly, it is observed that the antiferromagnetic spin orientation accumulates Δ_5 states close to the center of the BZ, while dispersing the Δ_1 states around the edges. It is apparent that (i) improvement in $k_{\|}$-integrated transmission can be induced by mixing of dispersed Δ_1 states in one of the Mn-atoms with Δ_1 states in Ir-atoms and (ii) mixing of accumulated Δ_5 states in one of the Mn-atoms with Δ_1 states in Ir-atoms induces improvement in transmission at $k_{\|}$= (0,0). This feature can be observed in panels (a) and (b) of Fig. 3. This confirms that the opposite spin orientation of the Mn-atoms is the central origin of symmetry-mixing that significantly improves the tunneling process in IrMn-MTJ.

Further, to intuitively understand how the antiferromagnetic spin orientation in IrMn may affect the traversing of an electron via the FeCo electrode by tunneling through the MgO barrier, we now analyze the density of states projected on every layer in the MTJ, along the direction of transport as plotted in Fig. 6. The electron for $P^{\uparrow\uparrow}$ or for $P^{\downarrow\downarrow}$ [see panels (a) and (b) of Fig. 6] encounters similar states on either side of the MgO barrier leading to a low resistance. On the other hand, due to dissimilar spin alignment, the states in FeCo are different on both sides of the MgO barrier for $AP^{\uparrow\downarrow}$ and for $AP^{\downarrow\uparrow}$ in panels (c) and (d) of Fig. 6, respectively. It is interesting to note that, the states in the outgoing IrMn also differ, particularly, that of the Mn atoms. This means that changing the spin alignment of the outgoing FeCo electrode, to achieve an antiparallel configuration, has also changed the behavior of antiferromagnetic IrMn. As a consequence, asymmetry in the potential of IrMn is observed in Fig. 1 panel (f). The asymmetry at FeCo/IrMn interface magnified in the inset of panel (f) of Fig. 1 validates the magnetically imbalanced interfaces. Microscopically, as seen in panels (c) and (d) of Fig. 6, neither the incoming nor the outgoing

IrMn or FeCo offer identical occupancy of states for AP alignment. Therefore, different transmission distributions are seen in panels (c) and (d) of Fig. 5.

Finally, we study the non-equilibrium behavior of tunneling by understanding I–V curve in the bias (V_b) range of 10 to 50 mV as displayed in Fig. 7. It is seen that the total current for P, I_P^{tot} is governed by the $I^{\uparrow\uparrow}$, while $I^{\downarrow\downarrow}$ is completely suppressed, resulting in a better spin filtering efficiency (SFE) that is not disturbed by antiferromagnetic spin orientation in the IrMn layer [see panel (a) of Fig. 7]. Specifically, in panel (b) of Fig. 7, $I^{\uparrow\downarrow}$ is entirely distinct from $I^{\downarrow\uparrow}$ for all V_b, which confirms the non-identical behavior of AP, discussed earlier. The total currents for P (I_P^{tot}) and AP (I_{AP}^{tot}) show a rather large difference leading to a large TMR of ∼8643%, which gradually descends with increasing V_b as seen in Fig. 7 panel (c). This non-equilibrium TMR is defined as TMR = $(I_P^{tot} - I_{AP}^{tot})/I_{AP}^{tot}$ with the total currents I_P^{tot} and I_{AP}^{tot} being the sum of spin-decomposed currents, such as $I_P^{tot} = I^{\uparrow\uparrow} + I^{\downarrow\downarrow}$ for P. With vanishing currents, the TMR at $V_b = 0$ is calculated using conductance at equilibrium.[39] In addition, the magnitude of the output signal in Fig. 7 panel (d) defined as $V_{out} \equiv V_b(R_P - R_{AP})/R_{AP}$ increases linearly with unhindered SFE of ∼99% [inset in panel (d) of Fig. 7]. SFE is defined as SFE = $(I^{\uparrow\uparrow} - I^{\downarrow\downarrow})/(I^{\uparrow\uparrow} + I^{\downarrow\downarrow})$ for P. These results suggest that an AFM IrMn layer can offer improvement of TMR, without hampering the spin-filtering effect. Furthermore, in AP [see Fig. 7 panel (b)], the non-identical feature displayed by $I^{\uparrow\downarrow}$ and $I^{\downarrow\uparrow}$ for all V_b validates the distinguishing transmission distribution in panels (c) and (d) of Fig. 5. It describes that a strong spin polarization appears in AP, which further provides guidance to realize and tune multiple resistance levels in IrMn-MTJ. Our MTJ structure can be ostensibly transformed into a multi-bit SOT-MTJ with appending IrMn layers acting as dual "*write*" channel layers.

IV. CONCLUSION

To summarize, the impact of an antiferromagnetic IrMn layer on the tunneling transport is investigated in the IrMn/FeCo/MgO/FeCo/IrMn magnetic tunnel junction, using a first-principles study. We show that the antiferromagnetically opposite spins of Mn atoms induce a Bloch symmetry-mixed tunneling over 2D-BZ. As a result, the tunneling in both the majority- and minority-spin channels in P improves, and a large TMR is obtained (up to 8640%). The non-identical transmission probabilities for $AP^{\uparrow\downarrow}$ and $AP^{\downarrow\uparrow}$, the asymmetry in the electrostatic potential profile, and the distinguishable $I^{\uparrow\downarrow}$ from $I^{\downarrow\uparrow}$ for all V_b suggest a strong spin polarization in AP, aside from PC. This means that the resistance levels can be tuned and so does the TMR, depending on the AFM spin orientation in IrMn and FM spin alignment in FeCo. Thus, our results propose possibilities to improve TMR in SOT-MTJs with simplified device design. Moreover, it also paves the way to evolve multi-bit SOT-MTJs with dual "*write*" channels.

SUPPLEMENTARY MATERIAL

See the supplementary material for the charge density distribution of lead–CSR–lead and the sparsity patterns of the Hamiltonian matrix elements.

ACKNOWLEDGMENTS

S.C.K and W.Z. thank Jiaqi Zhou for her participation in the early stages of this work. This work was funded by the National Key R&D Program of China (No. 2018YFB0407602), the Beijing Municipal Science and Technology Project (No. Z201100004220002), the International Collaboration Project (No. B16001), and the Beihang Hefei Innovation Research Institute (Project No. BHKX-19-02). Shradha C. Koli acknowledges the China Scholarship Council (CSC) for financial support. Shradha C. Koli also gratefully acknowledges financial support from the Graduate School of Excellence Materials Science in Mainz (MAINZ), Germany. Parts of this research were conducted using the supercomputer Mogon and advisory services offered by Johannes Gutenberg University Mainz (hpc.uni-mainz.de), which is a member of the AHRP (Alliance for High-Performance Computing in Rhineland Palatinate, www.ahrp.info) and the Gauss Alliance e.V. We acknowledge the computing time granted on the supercomputer Mogon at Johannes Gutenberg University Mainz (hpc.uni-mainz.de) and computing time at Mogon supercomputers.

AUTHOR DECLARATIONS

Conflict of Interest

The authors have no conflicts to disclose.

Author Contributions

Shradha Chandrashekhar Koli: Conceptualization (equal); Formal analysis (equal); Investigation (equal); Methodology (equal); Visualization (equal); Writing – original draft (equal). **Bertrand Dupé:** Formal analysis (equal); Investigation (equal); Software (equal); Supervision (equal); Visualization (equal); Writing – original draft (equal); Writing – review & editing (equal).**Hangyu Zhou:** Writing – review & editing (equal). **Weisheng Zhao:** Funding acquisition (equal); Investigation (equal); Project administration (equal); Supervision (equal); Validation (equal).

DATA AVAILABILITY

The data that support the findings of this study are available from the corresponding author upon reasonable request.

REFERENCES

[1]J. Godinho, H. Reichlová, D. Kriegner, V. Novák, K. Olejník, Z. Kašpar, Z. Šobáň, P. Wadley, R. Campion, R. Otxoa *et al.*, "Electrically induced and detected Néel vector reversal in a collinear antiferromagnet," Nat. Commun. **9**, 4686 (2018).

[2]N. Djavid and R. K. Lake, "Electron transport through antiferromagnetic spin textures and skyrmions in a magnetic tunnel junction," Phys. Rev. B **102**, 024419 (2020).

[3]J. Tong, Y. Wu, L. Ruan, B. Yang, G. Xie, G. Qin, F. Tian, and X. Zhang, "Breaking the symmetry of spin-sublattices in antiferromagnet by interfacial tailoring in the L1-MnPt/NaCl/Fe junction," Appl. Phys. Lett. **119**, 172401 (2021).

[4]L. Šmejkal, A. B. Hellenes, R. González-Hernández, J. Sinova, and T. Jungwirth, "Giant and tunneling magnetoresistance in unconventional collinear antiferromagnets with nonrelativistic spin-momentum coupling," Phys. Rev. X **12**, 011028 (2022).

[5]S. Shim, M. Mehraeen, J. Sklenar, J. Oh, J. Gibbons, H. Saglam, A. Hoffmann, S. S.-L. Zhang, and N. Mason, "Unidirectional magnetoresistance in antiferromagnet/heavy-metal bilayers," Phys. Rev. X **12**, 021069 (2022).
[6]D.-F. Shao, Y.-Y. Jiang, J. Ding, S.-H. Zhang, Z.-A. Wang, R.-C. Xiao, G. Gurung, W. Lu, Y. Sun, and E. Y. Tsymbal, "Néel spin currents in antiferromagnets," Phys. Rev. Lett. **130**, 216702 (2023).
[7]S. Fukami, C. Zhang, S. DuttaGupta, A. Kurenkov, and H. Ohno, "Magnetization switching by spin-orbit torque in an antiferromagnet–ferromagnet bilayer system," Nat. Mater. **15**, 535–541 (2016).
[8]Y.-W. Oh, S.-H. C. Chris Baek, Y. M. Kim, H. Y. Lee, K.-D. Lee, C.-G. Yang, E.-S. Park, K.-S. Lee, K.-W. Kim, G. Go, J.-R. Jeong, B.-C. Min, H.-W. Lee, K.-J. Lee, and B.-G. Park, "Field-free switching of perpendicular magnetization through spin-orbit torque in antiferromagnet/ferromagnet/oxide structures," Nat. Nanotechnol. **11**, 878–884 (2016).
[9]J. Zhou, X. Wang, Y. Liu, J. Yu, H. Fu, L. Liu, S. Chen, J. Deng, W. Lin, and X. Shu *et al.*, "Large spin-orbit torque efficiency enhanced by magnetic structure of collinear antiferromagnet IrMn," Sci. Adv. **5**, eaau6696 (2019).
[10]C. O. Avci, K. Garello, C. Nistor, S. Godey, B. Ballesteros, A. Mugarza, A. Barla, M. Valvidares, E. Pellegrin, A. Ghosh, I. M. Miron, O. Boulle, S. Auffret, G. Gaudin, and P. Gambardella, "Fieldlike and antidamping spin-orbit torques in as-grown and annealed Ta/CoFeB/MgO layers," Phys. Rev. B **89**, 214419 (2014).
[11]C. Zhang, S. Fukami, H. Sato, F. Matsukura, and H. Ohno, "Spin-orbit torque induced magnetization switching in nano-scale Ta/CoFeB/MgO," Appl. Phys. Lett. **107**, 012401 (2015).
[12]C.-F. Pai, L. Liu, Y. Li, H. Tseng, D. Ralph, and R. Buhrman, "Spin transfer torque devices utilizing the giant spin Hall effect of tungsten," Appl. Phys. Lett. **101**, 122404 (2012).
[13]S. Cho, S.-H. C. Baek, K.-D. Lee, Y. Jo, and B.-G. Park, "Large spin Hall magnetoresistance and its correlation to the spin-orbit torque in W/CoFeB/MgO structures," Sci. Rep. **5**, 1–9 (2015).
[14]S. Isogami, Y. Shiokawa, A. Tsumita, E. Komura, Y. Ishitani, K. Hamanaka, T. Taniguchi, S. Mitani, T. Sasaki, and M. Hayashi, "Spin–orbit torque driven magnetization switching in W/CoFeB/MgO-based type-Y three terminal magnetic tunnel junctions," Sci. Rep. **11**, 1–8 (2021).
[15]Y. Liu, B. Zhou, and J.-G. Zhu, "Field-free magnetization switching by utilizing the spin Hall effect and interlayer exchange coupling of iridium," Sci. Rep. **9**, 325 (2019).
[16]M. Cubukcu, O. Boulle, M. Drouard, K. Garello, C. Onur Avci, I. Mihai Miron, J. Langer, B. Ocker, P. Gambardella, and G. Gaudin, "Spin-orbit torque magnetization switching of a three-terminal perpendicular magnetic tunnel junction," Appl. Phys. Lett. **104**, 042406 (2014).
[17]V. Krizakova, M. Perumkunnil, S. Couet, P. Gambardella, and K. Garello, "Spin-orbit torque switching of magnetic tunnel junctions for memory applications," J. Magn. Magn. Mater. **562**, 169692 (2022).
[18]W. H. Butler, "Tunneling magnetoresistance from a symmetry filtering effect," Sci. Technol. Adv. Mater. **9**, 014106 (2008).
[19]X. Zhang and W. Butler, "Band structure, evanescent states, and transport in spin tunnel junctions," J. Phys.: Condens. Matter **15**, R1603 (2003).
[20]D. Odkhuu, S. Rhim, N. Park, and S. Hong, "Extremely large perpendicular magnetic anisotropy of an Fe (001) surface capped by 5D transition metal monolayers: A density functional study," Phys. Rev. B **88**, 184405 (2013).
[21]S. Peng, M. Wang, H. Yang, L. Zeng, J. Nan, J. Zhou, Y. Zhang, A. Hallal, M. Chshiev, and K. L. Wang *et al.*, "Origin of interfacial perpendicular magnetic anisotropy in MgO/CoFe/metallic capping layer structures," Sci. Rep. **5**, 1–6 (2015).
[22]D. Odkhuu, "Giant strain control of magnetoelectric effect in Ta—Fe—MgO," Sci. Rep. **6**, 32742 (2016).
[23]J. Zhou, W. Zhao, Y. Wang, S. Peng, J. Qiao, L. Su, L. Zeng, N. Lei, L. Liu, and Y. Zhang *et al.*, "Large influence of capping layers on tunnel magnetoresistance in magnetic tunnel junctions," Appl. Phys. Lett. **109**, 242403 (2016).
[24]S. Peng, D. Zhu, W. Li, H. Wu, A. J. Grutter, D. A. Gilbert, J. Lu, D. Xiong, W. Cai, P. Shafer, K. L. Wang, and W. Zhao *et al.*, "Exchange bias switching in an antiferromagnet/ferromagnet bilayer driven by spin–orbit torque," Nat. Electron. **3**, 757–764 (2020).
[25]X.-G. Zhang and W. Butler, "Large magnetoresistance in bcc Co/MgO/Co and FeCo/MgO/FeCo tunnel junctions," Phys. Rev. B **70**, 172407 (2004).
[26]J. Hafner, "*Ab – initio* simulations of materials using VASP: Density-functional theory and beyond," J. Comput. Chem. **29**, 2044–2078 (2008).
[27]L. Pál, E. Krén, G. Kádár, P. Szabó, and T. Tarnóczi, "Magnetic structures and phase transformations in Mn-based Cu-I type alloys," J. Appl. Phys. **39**, 538–544 (1968).
[28]H. Fuke, Y. Kamiguchi, S. Hashimoto, T. Funayama, K. Saito, H. Iwasaki, and M. Sahashi, "Exchange coupling film and magnetoresistive element," U.S. patent 6,057,049 (2 May 2000).
[29]K. Brun, A. Kjekshus, and W. Pearson, "Equiatomic transition metal alloys of manganese," Acta Chem. Scand. **19**, 107–112 (1965).
[30]Z. Lu, S.-H. Wei, A. Zunger, S. Frota-Pessoa, and L. Ferreira, "First-principles statistical mechanics of structural stability of intermetallic compounds," Phys. Rev. B **44**, 512 (1991).
[31]P. Ravindran, A. Kjekshus, H. Fjellvåg, P. James, L. Nordström, B. Johansson, and O. Eriksson, "Large magnetocrystalline anisotropy in bilayer transition metal phases from first-principles full-potential calculations," Phys. Rev. B **63**, 144409 (2001).
[32]J. Zhou, X. Shu, Y. Liu, X. Wang, W. Lin, S. Chen, L. Liu, Q. Xie, T. Hong, P. Yang, B. Yan, X. Han, and J. Chen, "Magnetic asymmetry induced anomalous spin-orbit torque in IrMn," Phys. Rev. B **101**, 184403 (2020).
[33]R. Umetsu, M. Miyakawa, K. Fukamichi, and A. Sakuma, "Pseudogap in the density of states and the highest Néel temperature of the $L1_0$-type MnIr alloy system," Phys. Rev. B **69**, 104411 (2004).
[34]S. Wang, A. Kohn, C. Wang, A. Petford-Long, S. Lee, R. Fan, J. Goff, L. Singh, Z. Barber, and R. Ward, "Exchange bias in epitaxial $Fe/Ir_{0.2}Mn_{0.8}$ bilayers grown on MgO (001)," J. Phys. D: Appl. Phys. **42**, 225001 (2009).
[35]C. Yang and C. Lai, "Exchange anisotropy in epitaxial (001) Co50Fe50/IrMn system," in *2006 IEEE International Magnetics Conference (INTERMAG)* (IEEE, 2006), pp. 579–579.
[36]J. D. Burton, S. S. Jaswal, E. Y. Tsymbal, O. Mryasov, and O. Heinonen, "Atomic and electronic structure of CoFeB/MgO interface from first principles," Appl. Phys. Lett. **89**, 142507 (2006).
[37]J. Taylor, H. Guo, and J. Wang, "*Abinitio* modeling of quantum transport properties of molecular electronic devices," Phys. Rev. B **63**, 245407 (2001).
[38]Y. Cai, Z. Bai, M. Yang, and Y. P. Feng, "Effect of interfacial strain on spin injection and spin polarization of $Co_2CrAl/NaNbO_3/Co_2CrAl$ magnetic tunneling junction," Europhys. Lett. **99**, 37001 (2012).
[39]D. Waldron, L. Liu, and H. Guo, "*Abinitio* simulation of magnetic tunnel junctions," Nanotechnology **18**, 424026 (2007).